Available online at www.sciencedirect.com
ScienceDirect
Earth and Planetary Science Letters 252 (2006) 245–259
EPSL
www.elsevier.com/locate/epsl

Deformation and melt transport in a highly depleted peridotite massif from the Canadian Cordillera: Implications to seismic anisotropy above subduction zones

Andréa Tommasi *, Alain Vauchez, Marguerite Godard, France Belley [1]

Laboratoire de Tectonophysique, CNRS and Université Montpellier II, 34095 Montpellier cedex 5, France

Received 3 July 2006; received in revised form 20 September 2006; accepted 20 September 2006
Available online 13 November 2006
Editor: C.P. Jaupart

Abstract

Seismic anisotropy in subduction zones results from a combination of various processes. Although it depends primarily on the orientation of olivine in response to flow, the presence of water and melt in the wedge may modify the deformation of olivine. The melt distribution also influences anisotropy. Direct observations of the deformation and melt-rock interactions in a strongly depleted spinel-harzburgite massif from the Cache Creek terrane in the Canadian Cordillera allow evaluating the relative contribution of each process. Structural mapping shows that this massif has recorded high-temperature, low-stress deformation, high degrees of partial melting, and synkinematic melt-rock interaction at shallow depths (<70 km) in the mantle, probably above an oblique subduction. Deformation, marked by shallow-dipping lineations and steep foliations, controlled melt distribution: reactive dunites and pyroxenite dykes are dominantly parallel to the foliation. Analysis of olivine crystal preferred orientations (CPO) indicates deformation by dislocation creep with dominant [100] glide. Glide planes are however different in harzburgites and dunites, suggesting that higher melt contents may favor glide on (001) relative to (010). Seismic properties, calculated by considering explicitly the large-scale structure of the massif, the olivine and pyroxene CPO, and possible melt distributions, show that the strain-induced olivine CPO results in up to 5% P- and S-wave anisotropy with fast seismic directions parallel to the lineation. Synkinematic melt transport by diffuse porous flow leading to melt pockets or dykes aligned in the foliation may significantly enhance this anisotropy, in particular for S-waves. In contrast, focused melt flow is not recorded by seismic anisotropy, unless associated with very high instantaneous melt fractions. Orientation of pyroxenite dykes suggests that the present orientation of the structures is representative of the pre-obduction situation, implying trench-parallel fast polarizations and high delay times as observed above the Kurils, Ryukyu, Taiwan, and Tonga subductions.

Keywords: subduction; seismic anisotropy; deformation; olivine; melt transport; upper mantle

1. Introduction

Seismic anisotropy data in subduction zones, in particular splitting measurements using local shear waves, show complex patterns. Fast shear wave polarization directions often vary over short wavelengths from parallel to normal to the trench, as observed in

* Corresponding author.
E-mail address: deia@dstu.univ-montp2.fr (A. Tommasi).
[1] Now at Earth Sciences, South Illinois University, Carbondale, IL 62901, USA.

0012-821X/$ - see front matter © 2006 Elsevier B.V. All rights reserved.
doi:10.1016/j.epsl.2006.09.042

the Andes [1,2], in the Kurils–Japan–Izu Bonin system [3–5], or in New Zealand [6]. Do these variations reflect changes in the mantle flow pattern along the subduction or with increasing distance from the trench and, hence, variable coupling of the mantle to the sinking slab? Or do they indicate a change in the mechanism responsible for the seismic anisotropy?

Seismic anisotropy in the mantle wedge above a subduction results from a combination of various processes. It depends primarily on the orientation of olivine crystals in response to flow in the mantle [7–10]. The presence of water and melt or higher stresses in the vicinity of the slab may change the dominant glide direction of olivine from [100] to [001], producing fast shear wave polarizations normal to the shear direction [11]. However, the actual water content of olivine in the mantle wedge and its effect on olivine deformation are still poorly constrained. Deformation partitioning in a partially molten mantle may also result in fast shear wave polarization normal to the flow direction [12]. In addition, partial melting may modify significantly the seismic anisotropy pattern in the mantle wedge if melt is concentrated in preferentially oriented disk-shaped pockets or cracks [13–15]. The seismic anisotropy will depend therefore on the melt transport processes (diffuse or focused porous flow, hydraulic fracturing…) and on their relation to deformation.

Insights on deformation and melt transport processes in the mantle and on their effect on seismic anisotropy may be obtained from the analysis of mantle slices tectonically emplaced on convergent margins (e.g., [16]). We present here a petrophysical study of a highly depleted spinel-harzburgite massif from the Cache Creek terrane in the Canadian Cordillera, which has recorded high degrees of partial melting and synkinematic melt-rock interaction at shallow depths in the mantle, probably above an oblique subduction. Structural mapping at the scale of the massif associated with analysis of the microstructure and of the olivine and pyroxene CPO allow determining the deformation pattern and the relation between deformation and melt distribution. Seismic properties are then calculated by considering explicitly the large-scale structure of the massif, olivine and pyroxene CPO, and different melt distributions. The predicted anisotropy is compared to shear wave splitting measurements performed above subduction zones.

2. The Murray Ridge peridotite massif

The Murray ridge massif is part of a series of peridotite massifs that outcrop within the Cache Creek terrane, an accretionary complex related to the Late Paleozoic — Early Mesozoic volcanic arcs of Quesnel and Stikine in the Canadian Cordillera (Fig. 1). These massifs, which are mainly composed by spinel-harzburgites, are traditionally interpreted as lower sections of dismembered ophiolite complexes [17]. Paleontologic assemblages in Cache Creek sediments and paleomagnetic data imply a large northward displacement of the Cache Creek terrane relative to the North American platform, suggesting that these mantle slices were accreted to the North American margin during a long-lived oblique convergence [18,19].

Murray Ridge is a 15 km long, 5 km wide peridotite body elongated in the N120°E direction, parallel to the Pinchi fault (Fig. 1). This dextral strike-slip fault is part of the Pinchi–Prince George fault system that separates the oceanic Cache Creek terrane from the arc-affinity Quesnel terrane. It has controlled the final emplacement of the peridotites as well as of slices of upper Carboniferous to Permian platform carbonates and upper Triassic blueschists within the Permian to lower Jurassic volcano-sedimentary sequences of the Cache Creek Complex [20].

The massif is essentially composed of spinel-harzburgites (70–80% olivine, 18–28% enstatite, 1–2% diopside, ≤1% spinel). Orthopyroxene contents are variable, but compositional banding is rare. Plagioclase-bearing facies were not observed. These spinel-harzburgites enclose frequent tabular (Fig. 2a) and fewer irregularly-shaped dunite bodies. Both tabular and irregular dunites display gradational contacts with the harzburgite (Fig. 2b). Tabular dunites may be followed over several meters and are generally 30–50 cm wide, although some may attain up to 1 m. They are systematically oriented N110–120°E subvertical. Their spacing varies within the massif from ~10 m in dunite-rich domains to more than 100 m in dunite-poor domains. The massif is also crosscut by numerous orthopyroxenite veins with sharp boundaries. These veins are usually a few cm wide, but some may attain up to 30 cm in width (Fig. 2c). They have variable orientations and are sometimes folded, but N120°E subvertical orientations dominate. Conjugate orthopyroxenite veins trending, respectively N110°E and N140°E, are also locally observed.

3. Chemical compositions: High-degree partial melting and melt-rock interaction in the shallow mantle

All Murray Ridge peridotites (harzburgites, dunites, and pyroxenites) display extremely refractory compositions: <2% clinopyroxene, highly magnesian compositions (whole rock Mg#=cationic Mg/(Fe+Mg)=91–92), very

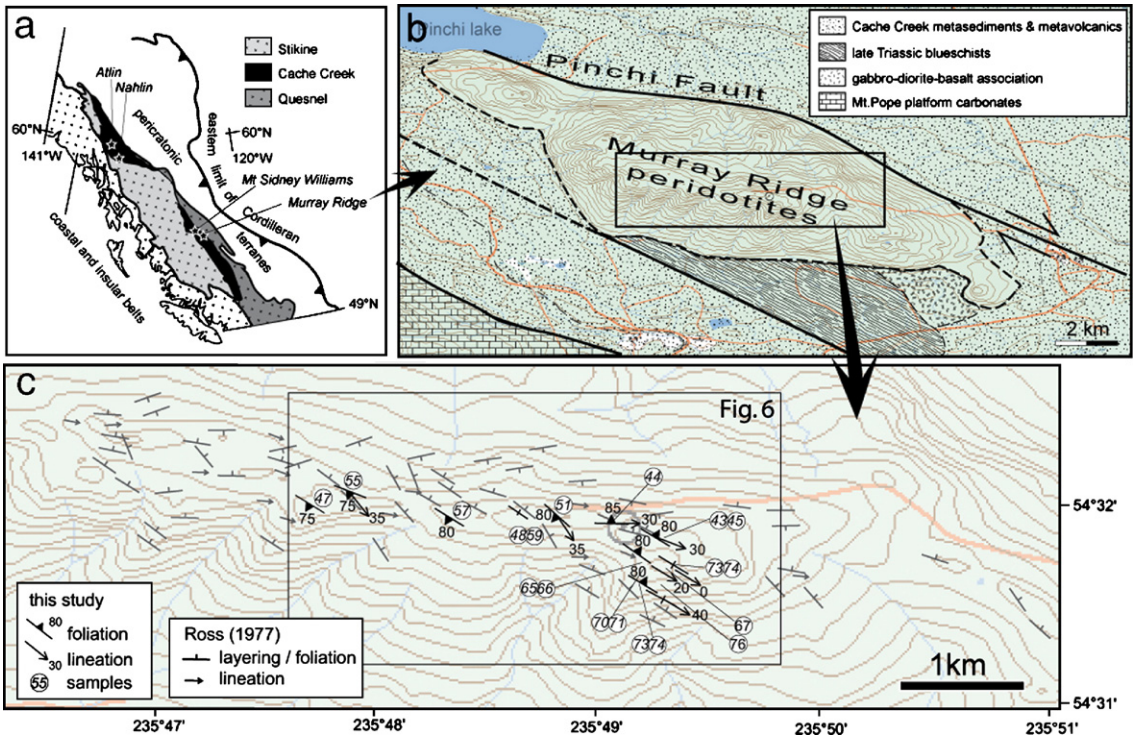

Fig. 1. (a) Ultramafic massifs (stars) outcropping in the Cache Creek terrane, an accretionary complex related to the Late Paleozoic–Early Mesozoic volcanic arcs of Quesnel and Stikine in the Canadian Cordillera. (b) Simplified geological map from the Murray Ridge area, modified from [20]. Due to forest cover, outcrops are limited to a 4 km long and 1 km wide NW–SE zone at the summit of the Murray Ridge, which represents the central part of the massif. (c) Structural map of the outcrop area, showing foliations and lineations determined in the present study and in [59] and the location of the samples for which crystal preferred orientations (CPO) were analyzed.

low Al contents (<0.5 wt.% Al_2O_3 in the harzburgites and <0.15 wt.% in the dunites), and Cr-rich spinels (Cr#=cationic Cr/(Cr+Al)=70–84) [21]. Trace-element compositions are strongly depleted: Yb contents, for instance, are ten to thirty times lower than chondritic compositions [21]. These highly refractory compositions can be reproduced by geochemical models of the evolution of modal and trace-element compositions during partial melting only for high degrees of melting (≥25% [21]).

The gradational contacts between dunites and harzburgites as well as similar Mg# and trace element compositions suggest a reactive origin for the dunites. Tabular dunites may have formed by either (i) diffusive reaction at the walls of melt-filled hydrofractures through focused melt percolation [22] or (ii) reactive melt percolation forming high porosity conduits [23,24]. Irregular dunite bodies probably represent domains that have interacted with higher melt fractions during porous flow.

In contrast, orthopyroxenite veins display clear-cut limits, which indicate that they represent short-lived melt-filled hydrofractures. Formation by brittle fracturing is also suggested by the conjugate character of some veins. Based on these structural relations and on their composition, we suggest that the orthopyroxenites represent crystallization products of Mg- and Si-rich, low Ca boninite-type melts [25]. These melts are usually interpreted as resulting from hydrous melting of refractory mantle rocks in subduction zones [26].

The refractory modal and chemical compositions of the Murray Ridge peridotites are similar to those observed in arc environments [27,28]. Together with the spatial association of the massif to blueschists and arc-derived assemblages, this suggests that these peridotites result from high degrees of melting in the shallow mantle above a subduction zone. The Murray Ridge massif is therefore a choice area to investigate the relations between partial melting, deformation, and melt transport in the mantle wedge.

4. Structural data: Synchronous deformation and melt-percolation

Harzburgites and dunites display a penetrative subvertical foliation with a consistent NW–SE trend and a shallowly dipping (0–40°) lineation towards

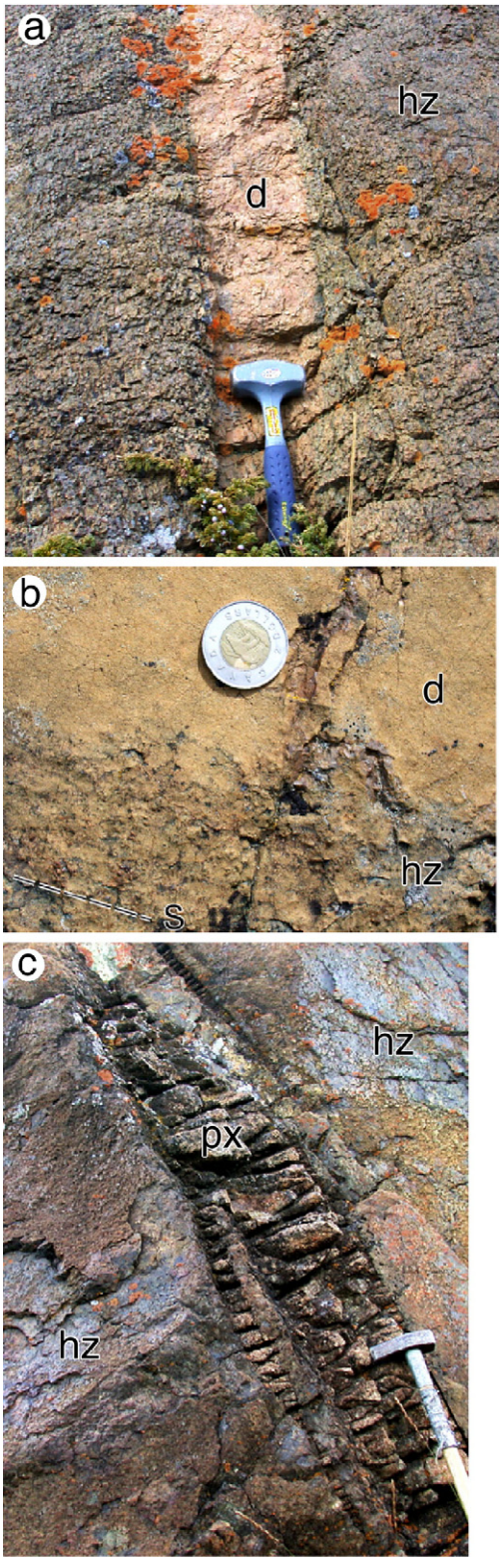

N120°E, which are marked by alignment of enstatite in the harzburgites (Fig. 2b) and of spinels in the dunites. This deformation seems to have controlled the structuration of the massif. Tabular dunites are systematically concordant and, although both concordant and discordant orthopyroxenite veins are observed, those parallel to the harzburgites foliation predominate. Assuming that, in the mantle above a subduction zone, melt migration is essentially a gravity-driven process, the dominant vertical orientation of tabular dunites and orthopyroxenite veins suggests that the present orientation of these structures in the massif corresponds to the original one in the wedge. In this case, shallowly-dipping lineations in the Murray Ridge peridotites record, similarly to those in peridotite massifs in the Talketna arc in Alaska [16], arc-parallel flow directions in the mantle wedge.

Microstructural analysis shows that deformation of the harzburgites and dunites took place under high-temperature, low-stress conditions. Both rocks display coarse-grained porphyroclastic textures characterized by large olivine grains (1–5 mm in the harzburgites and >1 cm in the dunites, Fig. 3), with widely spaced (100) subgrain boundaries and curved grain boundaries. Although xenomorphic, olivine and enstatite porphyroclasts usually display a weak shape preferred orientation that marks the foliation and lineation. Enstatite grains often show corrosion embayments filled by olivine (Fig. 3c), suggesting incongruent melting or orthopyroxene consuming melt-rock reactions, even in harzburgite samples collected tens of meters away from dunite bodies. Transition from harzburgite to dunite is characterized by progressive disappearance of enstatite and increase in olivine grain size.

Crystal preferred orientations (CPO) of olivine and enstatite were determined by indexation of electron backscattered diffraction (EBSD) patterns for 11 harzburgites, 6 dunites, and 2 dunite-harzburgite contacts (Figs. 4 and 5). Most harzburgites display a strong concentration of olivine [100] axes parallel to the lineation. [010] axes form a girdle normal to the lineation, with a maximum normal to the foliation. [001] axes are more dispersed. Some harzburgites display slightly weaker olivine CPO characterized by alignment of [010] normal to the foliation and dispersion

Fig. 2. (a) Tabular dunite (d), 20 cm wide, enclosed in coarse-grained harzburgite (hz). (b) Gradational contact between a tabular dunite (d) and the harzburgite (hz). Alignment of pyroxenes marks the foliation (dashed line, s) in the harzburgite. (c) Large orthopyroxenite (px) veins, up to 25 cm wide, showing sharp limits with the harzburgite (hz).

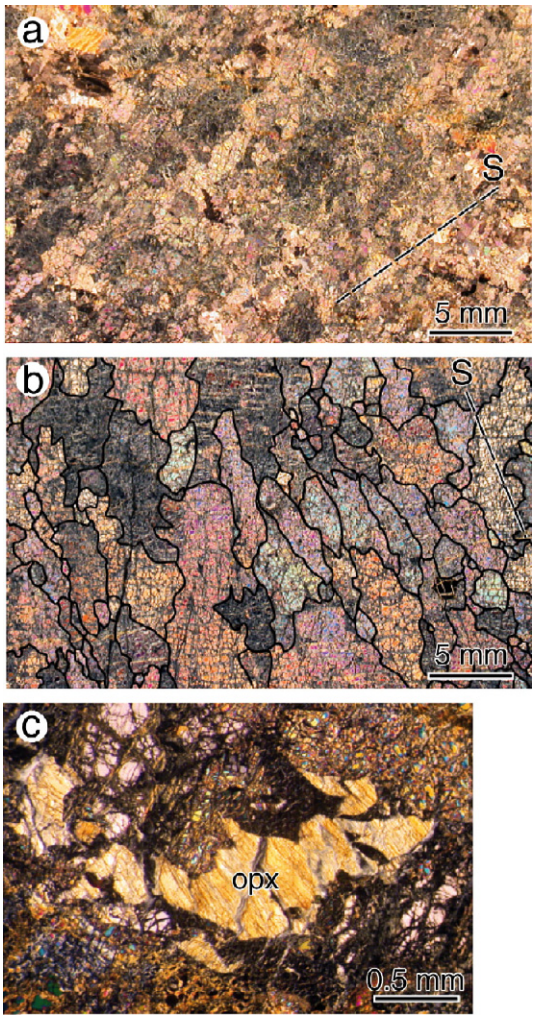

Fig. 3. Photomicrographs (crossed polarizers) illustrating typical microstructures in harzburgites and dunites. (a) High-temperature porphyroclastic microstructure in harzburgite. (b) Coarse-grained dunite showing highly lobated, interpenetrating olivine grain boundaries (hand-drawn for easier identification). (c) Orthopyroxene (opx) with corrosion embayments filled by olivine in a harzburgite. The foliation (dashed line, S) is marked by elongation of olivine porphyroclasts in both the harzburgite and the dunite. Scale is the same for (a) and (b), outlining the increase in grain size from the harzburgites to the dunites.

of [100] within the foliation plane. These CPO suggest that olivine deformation was accommodated essentially by dislocation glide on the high-temperature, low-pressure (0kl)[100] slip systems, with dominant activation of the (010) plane [10]. The dispersion of [100] within the foliation plane observed in some harzburgites may be due to either simultaneous activation of [100] and [001] slip systems or to a pure shear component in the deformation [29]. We favor the second hypothesis, i.e., local transpression, because in these samples enstatite also shows a dispersion of its dominant slip direction, [001], in the foliation plane.

Enstatite CPO in the harzburgites, although weak, is coherent with the olivine CPO (Fig. 4). [001] axes concentrate close to the lineation and [100] axes tend to align normal to foliation, suggesting activation of the high-temperature (100)[001] system. However, in most samples there is a small obliquity (<15°) between the olivine and enstatite CPOs. This obliquity suggests that although olivine and enstatite have suffered the same macroscopic deformation, the harder enstatite grains accommodated smaller strains. The inferred dextral shearing is coherent with the northward displacement of terranes along the Cordilleran margin [19], further suggesting that the present orientation of the structures in the massif corresponds to the original one in the wedge.

Olivine CPO in the dunites (Fig. 5) are significantly stronger than in the harzburgites. As in the former, [100] shows a strong concentration parallel to the lineation. However, in the dunites, [001] axes tend to align normal to the foliation and the [010] maximum is in the foliation plane. Finally, samples from harzburgite-dunite contacts show intermediate olivine CPO, in which [010] and [001] form an almost perfect girdle in a plane normal to the lineation. These CPO indicate that deformation in the dunites was accommodated essentially by dislocation glide on the high-temperature, low-pressure (0kl)[100] slip systems, with dominant glide on the (001) plane.

The stronger olivine CPO in the dunites may reflect either faster grain boundary migration or strain localization due to higher melt contents. Easier grain growth in the dunites is suggested by the grain size increase relatively to the harzburgites. The change in dominant glide plane from the usual high-temperature (010) plane to (001) may be related to a variation in chemical conditions, i.e., to higher water or oxygen fugacity [30,31] in the more permeable dunites relatively to the harzburgites [23,24]. Indeed, similar olivine CPO, suggesting dominant (001)[100] glide, although rare, have been described in refractory peridotites from island arc settings [16,32] and in dunites formed by melt-rock reactions in the crust-mantle transition zone of ophiolites [33–35]. The stronger CPO and the change in dominant slip system in the dunites, together with the preservation of the gradational contacts between harzburgites and dunites, suggest that melt percolation and high-temperature deformation were synchronous. This CPO evolution resulting from synkinematic melt transport contrasts with the one resulting from reactive melt percolation leading to olivine crystallization under

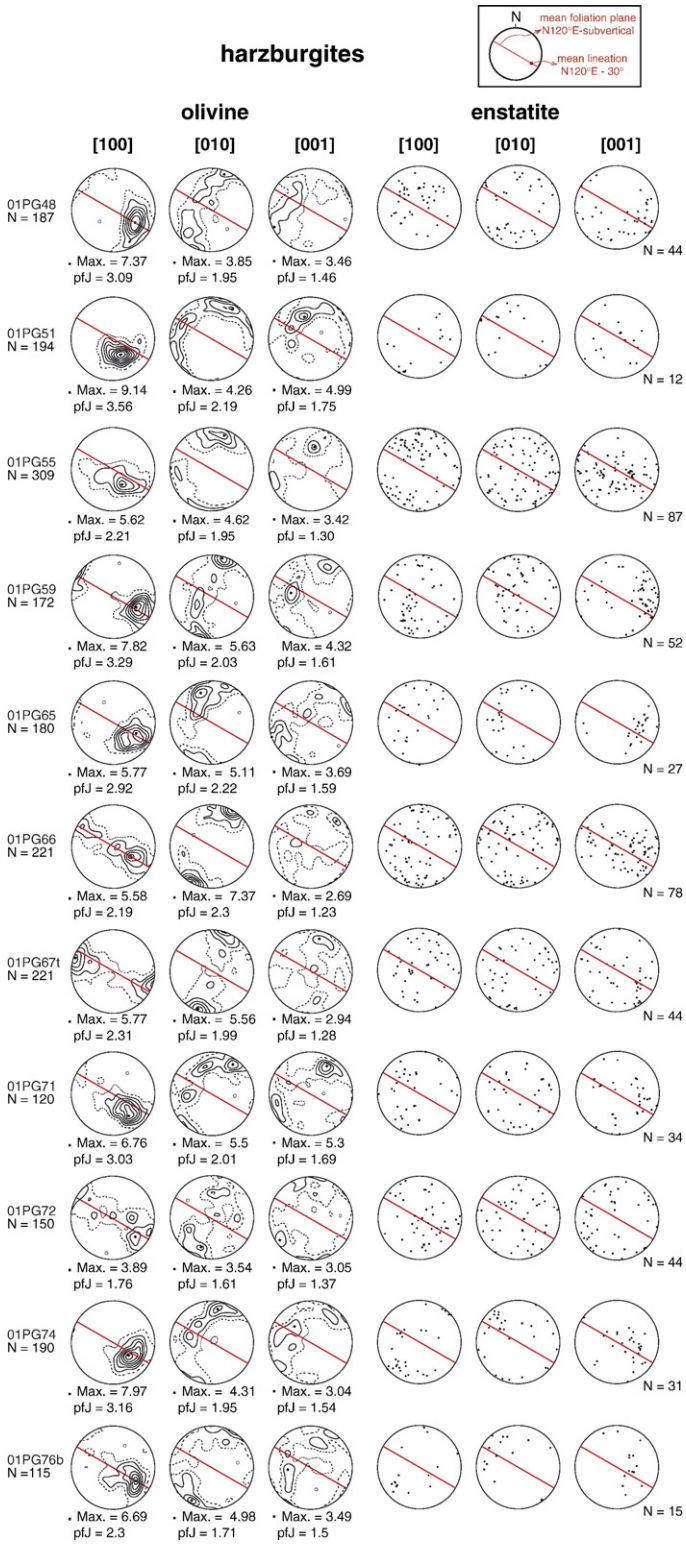

Fig. 4. Crystal preferred orientations (CPO) of olivine and enstatite in harzburgites. Equal area lower hemisphere stereographic projections in a geographic reference frame (top insert). Contours at 1 multiple of a uniform distribution intervals. *N*: number of grains measured. Enstatite CPO were not contoured because less than 100 grains could be measured in a thin-section. Full line represents the average orientation of the foliation in the massif (N120°-vertical).

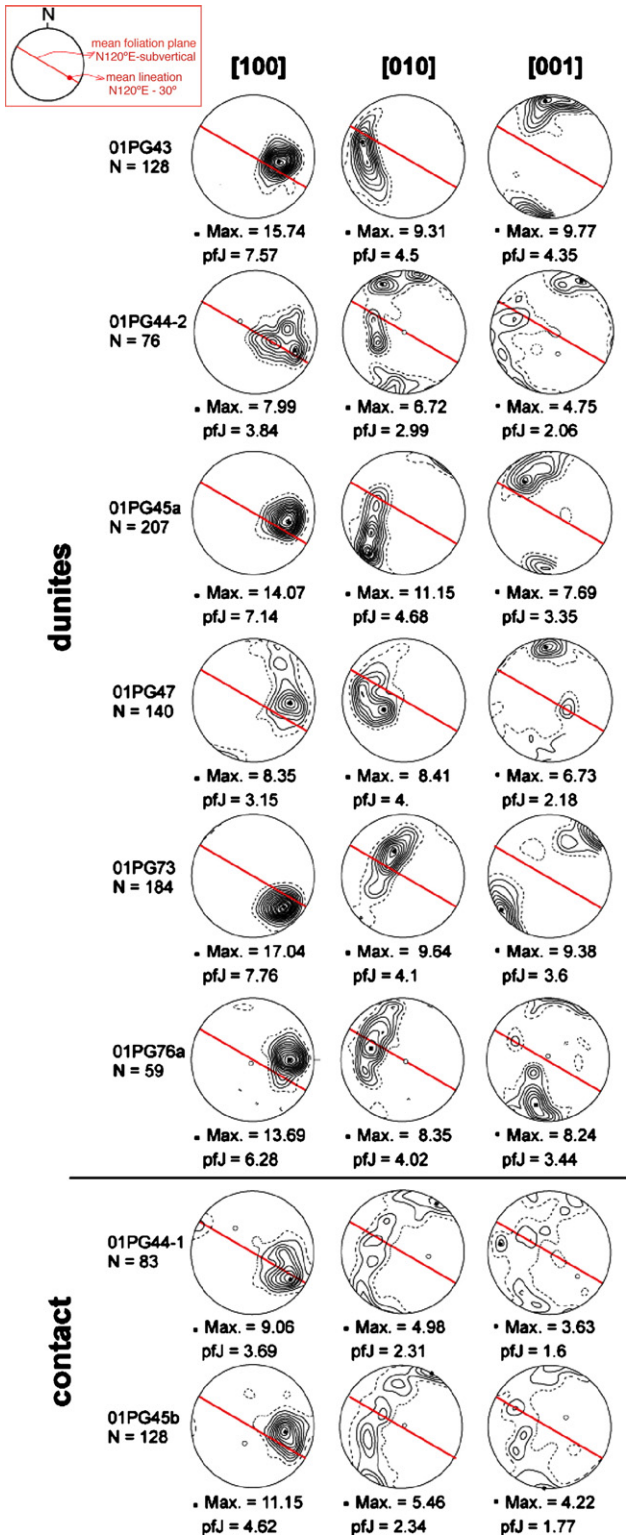

Fig. 5. Crystal preferred orientations (CPO) of olivine in dunites and at harzburgite-dunite gradational contacts. Equal area lower hemisphere stereographic projections in a geographic reference frame (top insert). Contours at 1 multiple of a uniform distribution intervals; square marks the maximum concentration. N: number of grains measured. pfJ is a measure of the intensity of the orientation of the crystallographic axis. Full line represents the average orientation of the foliation in the massif (N120°-vertical).

static conditions in French Polynesia, where the dunites show a clear weakening of olivine CPO relatively to the lherzolites and harburgites [36].

5. Seismic anisotropy: The effect of CPO and partial melt

5.1. CPO-induced seismic anisotropy

Seismic properties were estimated by averaging the individual grain elastic constants tensor as a function of the crystallographic orientation and modal composition. This method allows the calculation of the three-dimensional distribution of seismic velocities in an anisotropic polycrystalline aggregate [37]. In the present calculations, we used Voigt–Reuss–Hill averaging of the single-crystal elastic constant tensors of olivine and enstatite at 1200 °C and 1 GPa [38–40].

Seismic waves sample the anisotropy at length scales ranging from a few to a thousand of kilometer. Thus to average local, small-scale variations in the orientation of the foliation and lineation (Fig. 6), we calculate seismic properties for average harzburgite and dunite samples, obtained by summation of the crystal preferred orientations of individual samples. The weaker olivine CPO and the presence of orthopyroxenes result in lower anisotropy for the average harzburgite relatively to the dunite (Fig. 7). In addition, the two average samples show different CPO symmetries and, hence, different seismic velocity patterns. Both the harzburgite and the dunite show fast P-wave propagation and S-wave polarization parallel to the lineation. However, minimum P-wave velocities are normal to the foliation in the harzbugite and within the foliation for the dunite. S-waves velocity distributions and anisotropy patterns also differ. S-wave splitting is minimum for waves propagating normal to the foliation in the harzburgite and parallel to the lineation in the dunite.

Harzburgites form 97–98% of the massif. The properties of the average harzburgite are therefore a good estimate of the anisotropy at the scale of massif. Because of their small relative volume (2–3%), the dunite layers, although they display a higher anisotropy and a different S-wave splitting pattern, do not significantly modify the large-scale anisotropy. They produce only a very small increase in anisotropy intensity (<0.2%). Even in presence of larger amounts of dunites (up to 20 vol.%) seismic anisotropy is still controlled by the harzburgites' composition and CPO. Thus if, as suggested by the vertical orientation of the tabular dunites and pyroxenite dykes, the present orientation of the massif is representative of the original one in the mantle wedge, P-waves velocities are fastest for horizontal propagation parallel to the massif elongation (N120°E), i.e., parallel to the trench, and slowest for horizontal propagation normal to it. Fast SKS waves will be polarized parallel to the trench and delay times will be large. Surface waves polarization anisotropy varies strongly with the backazimuth; it is maximum parallel to the trench with SV faster than SH and no anisotropy is observed for propagation normal to the trench. Rayleigh waves propagation anisotropy is strong (4%); the fastest propagation is also parallel to the trench.

5.2. Melt distribution and seismic anisotropy

The seismic properties of the fully-crystallized samples are representative of the present-day peridotite massif, i.e., of a fossil partial melting domain. To evaluate the seismic anisotropy signature of an active mantle wedge, we have to infer the melt fraction and its distribution.

The composition and structure of the dunites suggest that they formed by reactive melt percolation in the harzburgites. Tabular dunites are predominant in the massif. They represent layers parallel to the foliation that were percolated by higher amounts of melt during the evolution of the mantle section. Yet seismic measurements are not sensitive to the melt fraction integrated in time, but to the instantaneous melt fraction. If the dunites formed by diffusive reaction around melt-filled dykes [22], they mark the emplacement of the dykes, i.e., of 100% melt domains with very flattened shapes (aspect ratios $\geq$50:50:1). On the other hand, if the dunites formed by reactive melt percolation [23,24], they represent higher permeability, but not necessarily higher porosity domains. However, simulations of the development of reactive melt instabilities suggest that compaction and melt focusing lead to higher porosity in the dunite channels (1–4%) relatively to the matrix (0.1%) [41].

Corrosion of pyroxenes in the harzburgites implies that they were also percolated by small melt fractions. Elongation of corroded pyroxenes suggests preferential melt migration parallel to the foliation. This observation is in good agreement with static experiments in olivine-basalt systems showing that the anisotropy of surface energy in olivine leads to preferential concentration of melt in disk-shaped inclusions along (010) grain boundaries [42,43]. In the harzburgites, (010) olivine faces are indeed oriented preferentially parallel to the foliation (Fig. 4). Moreover, shear experiments on partially molten aggregates show that deformation enhances grain boundary wetting and may even lead to segregation of melt in bands parallel or at low angle to

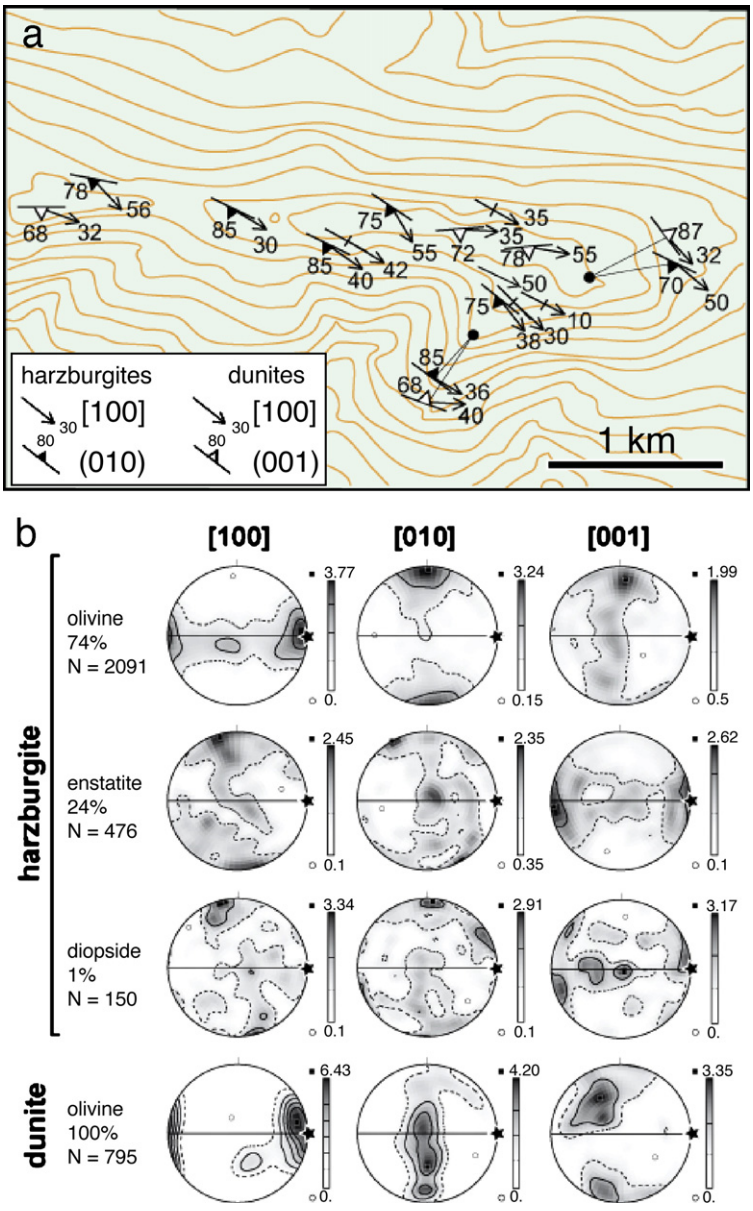

Fig. 6. (a) Map of the crystallographic fabrics in the Murray Ridge massif. For each sample, the arrow shows the preferred orientation of the olivine main glide direction: [100], and the foliation symbol marks the preferred orientation of the main glide plane: (010) in the harzburgites and (001) in the dunites. (b) Average olivine, enstatite, and diopside CPO for the harzburgites and olivine CPO for the dunites obtained by summation of the CPO of individual samples. Full line represents the mean orientation of the foliation in the massif (N120°E-subvertical) and the star the mean orientation of the lineation, which dips by 35° towards N120°E.

the shear plane [44,45]. Finally, orthopyroxenite veins represent melt-filled dykes, which formed probably during a later stage of the evolution of the mantle section. These dykes show a preferential orientation parallel to the high-temperature foliation (N120°E subvertical). However, their small proportion in volume (<1%) probably limits their influence on the seismic properties at the scale of the mantle section.

Based on these observations, we have calculated, using a method that associates the Gassman poro-elastic approach at low frequencies with a differential effective medium approach at high frequencies [14], the seismic properties of:

1- A harzburgitic massif displaying up to 2% melt in isometric or disk-shaped pockets elongated parallel to

the foliation with aspect ratios varying from 2:2:1 to 50:50:1 (Fig. 8). The low aspect ratio models allow evaluating the effect of an anisotropic porous flow in the harzburgites and the highest aspect ratio models, the effect of melt-filled dykes.

2- A harzburgitic massif containing <1% distributed melt interlayered with tabular dunites (1–5% in volume and aspect ratios of 50:50:1) containing up to 5% melt in disk-shaped inclusions with aspect ratios varying from 2:2:1 to 50:50:1 (Fig. 9). These models allow evaluating the effect of focused melt flow in reactional dunite channels on seismic anisotropy.

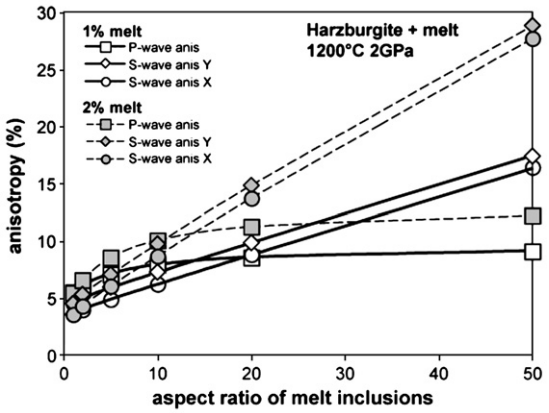

Fig. 8. Variation of the maximum P-wave propagation anisotropy (A%= 200*(VPmax−VPmin)/(VPmax+VPmin), squares) and S-wave polarization anisotropy for waves propagating in the foliation parallel to the lineation (X, circles) and normal to it (Y, diamonds) in a partially molten harzburgitic mantle as a function of the aspect ratio of the melt inclusions for melt fractions of 1% (white symbols) and 2% (gray symbols).

Very weak melt fractions (≤1%) dispersed in a harzburgitic mantle do not significantly modify seismic velocities and anisotropy, unless melt occurs as strongly flattened inclusions (aspect ratios ≥5) (Fig. 8). Disk-shaped melt inclusions aligned in the foliation lower P-wave velocities normal to the flow plane, which contains the melt pockets, and hence increase the P-wave azimuthal anisotropy proportionally to the logarithm of the aspect ratio of the melt pockets. S-wave polarization anisotropy is still more sensitive to the shape of melt inclusions. Polarization anisotropy for S-waves propagating within the foliation increases linearly as a function of the aspect ratio of the melt pockets. For melt pockets with aspect ratios ≥20:20:1, which are a good approximation for oriented dykes, the S-wave polarization anisotropy shows a two-fold or more increase.

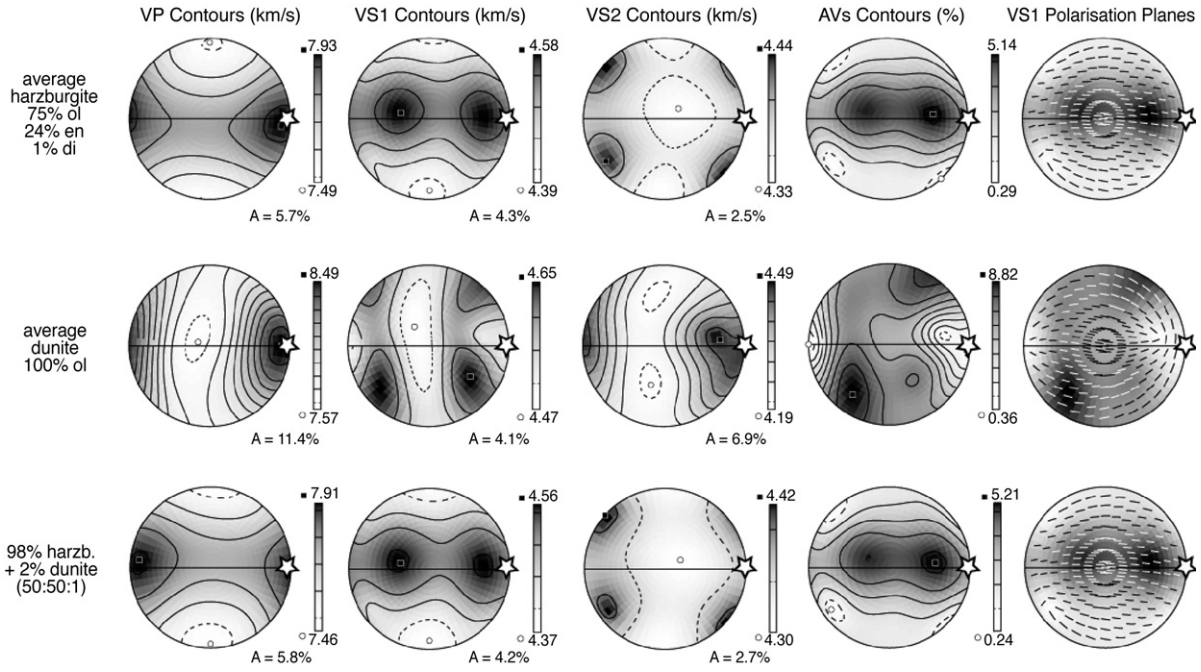

Fig. 7. Seismic properties of the average harzburgite and dunite and of a massif composed by harzburgites enclosing 2% of tabular dunites. From left to right, variation of the compressive (VP) and of the two quasi-shear waves (VS1 and VS2) velocities and shear wave polarization anisotropy: intensity (AVs%=200*(VS1−VS2)/*(VS1+VS2)) and polarization of the fast shear wave (S1) as a function of the propagation direction relative to the foliation plane (full line) and lineation (star). Equal area, lower hemisphere stereographic projections. Contours at 0.1 km/s and 0.05 km/s for P- and S-wave velocities, respectively.

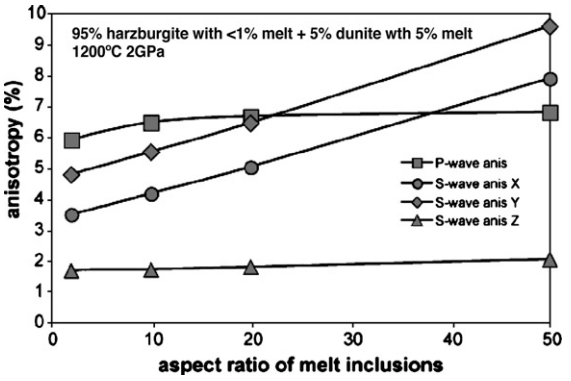

Fig. 9. Variation of the maximum P-wave propagation anisotropy (A% = 200 * (VPmax − VPmin) / (VPmax + VPmin), squares) and S-wave polarization anisotropy for waves propagating in the foliation parallel to the lineation (X, circles) and normal to it (Y, diamonds) in a harzburgitic mantle containing <1% distributed melt interlayered with tabular dunites (5% in volume and aspect ratios of 50:50:1) containing 5 vol.% of melt in disk-shaped inclusions with aspect ratios varying from 2:2:1 to 50:50:1.

S-waves propagating normal to the foliation are not affected by the presence of melt. At 2% melt fraction, both P- and S-wave anisotropies show a stronger dependence on the aspect ratio of melt pockets (Fig. 8). A two-fold increase is observed for aspect ratios as low as 10:10:1. S-waves azimuthal anisotropy is also doubled; fast S-waves propagate faster within the foliation and slower normal to it, slow S-waves propagate slower normal and parallel to the foliation and faster at 45° to the lineation (Fig. 10).

In contrast, focused melt flow in reactional dunitic channels, because it involves small instantaneous melt fractions (≤5%) in the dunites and, hence, very small total melt fractions (≤0.1%) in the massif, has no significant effect on seismic anisotropy unless the melt distribution in the dunites is extremely anisometric (aspect ratios ≥20 for 5% melt, Fig. 9). Porous flow may however produce such high aspect ratios. Static experiments on olivine + basalt aggregates equilibrated at 1 GPa and 1300–1400 °C show that, for melt fractions ≤3.3 vol.%, most melt concentrated in disk-shaped melt inclusions with 20:20:1 aspect ratios [42]. Deformation may further enhance the anisotropy of melt distribution [44]. Yet, even for the highest melt fractions (5%) and aspect ratios (50:50:1), P-wave propagation anisotropy increases by <1% and S-wave polarization anisotropy by ≤2% (Fig. 9).

6. Implications for seismic anisotropy above subduction zones

Strain-induced crystal preferred orientations in the Murray Ridge massif result in up to 5% P- and S-wave anisotropy with fast seismic directions parallel to the lineation, i.e., to the shear direction in the mantle. Waves propagating normal to the foliation display the lowest P- and S-wave velocities and no S-wave splitting. Synkinematic melt transport by either diffuse porous flow or fractures, resulting in melt pockets or dykes aligned in the foliation, does not modify the seismic anisotropy pattern, but enhances the anisotropy intensity, in particular for S-waves. On the other hand, focused porous flow in dunitic channels does not affect significantly seismic anisotropy, unless associated with very high instantaneous melt contents.

If the present orientation of the structures is representative of the pre-obduction situation, as suggested by the orientation of the tabular dunites and pyroxenite dykes and the kinematics deduced from olivine and enstatite CPO relationships, the Murray Ridge massif should be characterized by trench-parallel fast S-wave polarizations and variable delay times, depending on the S-wave incidence angle. How does this fossil seismic anisotropy pattern compare to observations above active subduction zones?

Shear wave splitting patterns observed in subduction zones are complex. Teleseismic shear wave

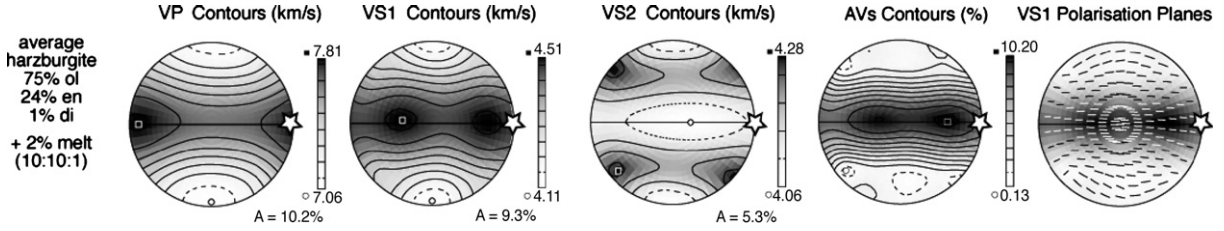

Fig. 10. Seismic properties of a harzburgite containing 2% melt in 10:10:1 lenses parallel to the foliation. From left to right, variation of the compressive (VP) and of the two quasi-shear waves (VS1 and VS2) velocities and shear wave polarization anisotropy: intensity (AVs% = 200 * (VS1 − VS2) / *(VS1 + VS2)) and polarization of the fast shear wave (S1) as a function of the propagation direction relative to the foliation plane (full line) and lineation (star). Equal area, lower hemisphere stereographic projections. Contours at 0.1 km/s and 0.05 km/s for P- and S-wave velocities, respectively.

splitting data show that trench-parallel fast polarization directions and high delay times (1–1.5 s) predominate along the circum-Pacific and Caribbean subductions. Clear trench-normal fast teleseismic S-wave polarizations are only observed in the Tonga and Marianas subductions [46] and the Cascades [47]. Moreover, many subduction zones, like the Andes [1] or the Izu Bonin–Japan–Kurils system [46], display polarization directions that vary from trench-parallel to trench-normal along the subduction. However, these measurements integrate the anisotropy produced by the orientation of olivine crystals due to flow below the slab, the frozen olivine CPO within the slab, and the anisotropy generated in the wedge. The relative contribution of each component may be inferred from the comparison with splitting data retrieved from local S-waves, which sample essentially the wedge and, depending on the source location, part of the slab.

Teleseismic and local S-waves splitting data are, in general, coherent. Trench-parallel polarizations are also predominant in local S-wave data, in particular in fore-arc and arc domains, as in the Aleutians–Alaska arc [48,49], in the Caribbean (M. Kendall, personal communication 2006), and in the southern Hikurangi subduction [6,50]. However, fast polarization directions for local S-waves are often more heterogeneous than SKS data. The more pronounced heterogeneity may partially be explained by the higher frequency of these waves, which results in larger scattering, and by the more variable source-receiver geometries (e.g., [1,3,5,6,51]). In the Andes [1] and the Kamchatka [51], local S-waves show indeed very weak anisotropy and highly variable polarization directions. However clear patterns are observed. Fast polarization of local S-waves varies over short wavelengths (<50 km), either along the subduction zone from parallel to normal to the local orientation of the trench, as in Izu Bonin [5], or with increasing distance from the trench. A large number of western Pacific subduction zones, like Ryukyu [4], Japan [3,5], the Tonga–Lau system [52], and the northern part of the Hikurangi subduction in New Zealand [6], show indeed dominant trench-parallel polarization of local S-waves in the fore-arc and trench-normal polarizations in the back-arc. These variations in the orientation of fast S-wave polarization have been interpreted as marking: (i) changes in the flow pattern, (ii) a transition from wet to dry olivine deformation, and (iii) the combination of different anisotropy sources (differently oriented olivine CPO in the wedge and the slab, aligned melt pockets…).

Analysis of the observed delay times may allow discrimination between these models. Olivine deformation by dominant [001] slip under water saturated conditions always results in weak orientation of the fast [100] axis and hence in weak anisotropy, leading to low delay times independent of the orientation of the flow plane [53]. In contrast, our results show that, in a wedge characterized by trench parallel flow and synkinematic melt transport, the anisotropy intensity sampled by high-angle S-waves depends on the orientation of the flow plane: steep foliations result in high delay times, subhorizontal foliations in very low delay times.

Delay times for local S-waves are usually ≤ 0.4 s [2,3,6,48,49,51]. Observation of such low delay times for deep events (epicenter depths >100 km) suggests weak S-wave anisotropy in the wedge (<2%). Our models (Figs. 7,9 and 10)) show that S-waves propagating oblique or normal ($\geq 30°$) to the flow plane sample low anisotropy (<2%) directions. As a consequence, both trench-parallel flow in subhorizontal planes and corner flow will result in low delay times. These two models however would result in fast polarizations parallel and normal to the trench, respectively. Dominant [001] slip in olivine would also produce low anisotropy, but the relation between fast seismic axes and flow would be inversed. In conclusion, the interpretation of these low delay time data is non-unique.

In contrast, high delay times (≥ 1 s) and fast polarizations implying large trench-parallel anisotropy in the mantle wedge are observed for local S-waves in the Kurils [54], Ryukyu [4], southwest Taiwan [55], and Tonga subductions [52]. These observations are fully consistent with the seismic anisotropy calculated for the Murray Ridge massif considering that the present orientation of the structures is representative of the pre-obduction situation, i.e., for trench-parallel flow and melt alignment in steeply-dipping planes.

Finally, an indirect consequence of the low delay times observed using local S-waves is that a large part of the SKS delay times results from olivine CPO orientation in response to flow beneath the slab. Trench-parallel fast SKS polarization directions and high delay times (1–1.5 s) observed in New Zealand, Kamchatka, Mediterranean, and Caribbean subductions imply trench-parallel flow and, hence, a strong decoupling between the downgoing slab and flow in the convective mantle. Different settings processes have been proposed to produce toroidal flow beneath slabs: trench retreat [1,56], a lateral discontinuity in the slab [51], oblique subduction [57], or transform-subduction interactions [58]. However, the processes allowing for mantle flow decoupled from the downgoing slab are still poorly understood.

7. Conclusion

A large range of arguments converge to point that the Murray Ridge peridotites represent a slice of the mantle wedge above an oblique subduction: its emplacement in an accretionary complex interleaved with island arc magmatic assemblages, the strongly depleted compositions of the peridotites, characteristic of high degree melting residues, the synkinematic transport of low-Ca boninitic magmas, as well as paleontological and paleomagnetic data suggesting belt-parallel transport during and after the accretion of the Cache Creek terrane to the western North America margin. This massif represents therefore a natural laboratory to investigate the relations between partial melting, deformation, and melt transport in the mantle wedge.

Structural mapping shows that it has recorded high-temperature, low-stress deformation, high degrees of partial melting, and synkinematic melt-rock interaction at shallow depths (<70 km) in the mantle. Deformation, marked by shallow-dipping lineations and steep foliations, controlled melt distribution: reactive dunites and pyroxenite dykes are dominantly parallel to the foliation. Analysis of olivine crystal preferred orientations (CPO) indicates that it deformed by dislocation creep with dominant [100] glide. Glide planes are however different in harzburgites and dunites, suggesting higher melt contents may favor glide on (001) relative to (010) in the dunites. The change in slip system and the stronger olivine CPO in the dunites, as well as the preservation of gradational contacts between dunites and harzburgites, imply that deformation and melt transport were synchronous.

Seismic properties, calculated by considering explicitly the large-scale structure of the massif, the olivine and pyroxene CPO, and possible melt distributions, show that the strain-induced olivine CPO results in up to 5% P- and S-wave anisotropy with fast seismic directions parallel to the lineation. Synkinematic melt transport by diffuse porous flow leading to melt pockets or dykes aligned in the foliation may significantly enhance this anisotropy, in particular for S-waves. On the other hand, focused melt flow in high permeability dunitic "channels" cannot be recorded by seismic anisotropy, unless it leads to very high melt concentrations (>10%).

The dominant vertical orientation of dunitic "channels" and pyroxenite dykes together with the dextral shear inferred from the comparison of olivine and enstatite CPO in the harzburgites suggest that the present orientation of the structures is representative of the pre-obduction situation. The seismic anisotropy resulting from high temperature deformation and synkinematic melt transport in the Murray Ridge massif is coherent with the trench-parallel fast S-wave polarizations and large delay times observed above the Kurils, Ryukyu, southwest Taiwan, and Tonga subductions. Delay times depends on the orientation of the flow plane relatively to the S-wave propagation. For waves with high incidence angles, steep and subhorizontal foliations result in strong and weak anisotropy, respectively. The low delay times observed above a large number of subduction zones using local S-waves may result therefore from various processes: (i) corner flow and trench-parallel flow in flat-lying planes in the wedge with normal [100] slip in olivine, (ii) olivine deformation by [001] slip, or (iii) complex relations between deformation and melt distribution. Their interpretation in terms of flow patterns in the wedge is therefore non-unique. In contrast, trench-parallel fast polarizations and high delay times are characteristic of trench-parallel flow in steeply dipping planes.

Acknowledgements

Work on the Murray Ridge massif was initially proposed by Henriette Lapierre, to whom this article is dedicated. She and Marc Tardy introduced the Murray Ridge massif to AT and AV. This study was funded by the Institut National des Sciences de l'Univers (CNRS/INSU) program "Intérieur de la Terre".

References

[1] R.M. Russo, P.G. Silver, Trench-parallel flow beneath the Nazca plate from seismic anisotropy, Science 263 (1994) 1105–1111.
[2] M.L. Anderson, G. Zandt, E. Triep, M. Fouch, S. Beck, Anisotropy and mantle flow in the Chile–Argentina subduction zone from shear wave splitting analysis, Geophys. Res. Lett. 31 (2004) L23608, doi:10.1029/2004GL020906.
[3] J. Nakajima, A. Hasegawa, Shear-wave polarization anisotropy and subduction-induced flow in the mantle wedge of northeastern Japan, Earth Planet. Sci. Lett. 225 (2004) 365–377.
[4] M.D. Long, R.D. van der Hilst, Shear wave splitting from local events beneath the Ryukyu arc: trench-parallel anisotropy in the mantle wedge, Phys. Earth Planet. Inter. 155 (2006) 300–312.
[5] D.K. Anglin, M.J. Fouch, Seismic anisotropy in the Izu-Bonin subduction system, Geophys. Res. Lett. 32 (2005) L09307.
[6] E. Audoine, M.K. Savage, K. Gledhill, Anisotropic structure under a back arc spreading region, the Taupo Volcanic zone, New Zealand, J. Geophys. Res. 109 (2004) B11305, doi:10.1029/2003JB002932.
[7] N.I. Christensen, R.S. Crosson, Seismic anisotropy in the upper mantle, Tectonophysics 6 (1968) 93–107.
[8] A. Nicolas, N.I. Christensen, Formation of anisotropy in upper mantle peridotites—A review, in: K. Fuchs, C. Froidevaux (Eds.), Composition, Structure and Dynamics of the Lithosphere–Asthenosphere System, vol. 16, Am. Geophys. Un., Washington, D.C., 1987, pp. 111–123.

[9] N.M. Ribe, Seismic anisotropy and mantle flow, J. Geophys. Res. 94 (1989) 4213–4223.
[10] A. Tommasi, D. Mainprice, G. Canova, Y. Chastel, Viscoplastic self-consistent and equilibrium-based modeling of olivine lattice preferred orientations. Implications for upper mantle seismic anisotropy, J. Geophys. Res. 105 (2000) 7893–7908.
[11] H. Jung, S.-I. Karato, Water-induced fabric transitions on olivine, Science 293 (2001) 1460–1463.
[12] B.K. Holtzman, D.L. Kohlstedt, M.E. Zimmerman, F. Heidelbach, T. Hiraga, J. Hustoft, Melt segregation and strain partitioning; implications for seismic anisotropy and mantle flow, Science 301 (2003) 1227–1230.
[13] J.M. Kendall, Teleseismic arrivals at a mid-ocean ridge: effect of mantle melt and anisotropy, Geophys. Res. Lett. 21 (1994) 301–304.
[14] D. Mainprice, Modelling anisotropic seismic properties of partially molten rocks found at mid-ocean ridges, Tectonophysics 279 (1997) 161–179.
[15] A. Vauchez, A. Tommasi, G. Barruol, J. Maumus, Upper mantle deformation and seismic anisotropy in continental rifts, Phys. Chem. Earth, Part A Solid Earth Geod. 25 (2000) 111–117.
[16] L. Mehl, B.R. Hacker, G. Hirth, P.B. Kelemen, Arc-parallel flow within the mantlewedge: evidence from the accreted Talkeetna arc, south central Alaska, J. Geophys. Res. 108 (2003) 2375, doi:10.1029/2002JB002233.
[17] J.G. Shellnutt, D. Canil, S.T. Johnston, Preliminary results of a petrological study of ultramafic rocks of the Northern Cordillera, in: D.S. Emond, L.H. Weston, L.L. Lewis (Eds.), Yukon Exploration and Geology 2001, Exploration and Geological Services Division, Yukon Region, Indian and Northern Affairs Canada, 2002, pp. 229–237.
[18] P.J. Coney, Cordilleran tectonics and North American plate motions, Am. J. Sci. 272 (1972) 462–465.
[19] J. Monger, R. Price, The Canadian Cordillera: geology and tectonic evolution, Canadian Society of Geophysicists Recorder, vol. 27, 2002, pp. 17–36.
[20] M. Tardy, H. Lapierre, L.C. Struik, D. Bosch, P. Brunet, The influence of mantle plume in the genesis of the Cache Creek oceanic igneous rocks: Implications for the geodynamic evolution of the inner accreted terranes of the Canadian Cordillera, Can. J. Earth Sci. 38 (2001) 515–534.
[21] I. Chane-fo, Fusion partielle et circulation de magmas dans le manteau supérieur: étude pétrologique et géochimique des péridotites réfractaires et pyroxénites du massif péridotitique de Murray Ridge, Canada, M.Sc., Univ. Montpellier II, 2002.
[22] A. Nicolas, A melt extraction model based on structural studies in mantle peridotites, J. Petrol. 27 (1986) 999–1022.
[23] E.J. Aharonov, P.B. Whitehead, P. Kelemen, M. Spiegelman, Channeling instability of upwelling melt in the mantle, J. Geophys. Res. 100 (1995) 20,433–420,450.
[24] P.B. Kelemen, H.J.B. Dick, Focused melt flow and localized deformation in the upper mantle; juxtaposition of replacive dunite and ductile shear zones in the Josephine Peridotite, SW Oregon, J. Geophys. Res. 100 (1995) 423–438.
[25] R.L. Hickey, F.A. Frey, Geochemical characteristics of boninite series volcanics: implications for their source, Geochim. Cosmochim. Acta 46 (1982) 2099–2115.
[26] T.J. Falloon, L.V. Danyushevsky, Melting of refractory mantle at 1.5, 2 and 2.5 GPa under anhydrous and H2O-undersaturated conditions; implications for the petrogenesis of high-Ca boninites and the influence of subduction components on mantle melting, J. Petrol. 41 (2000) 257–283.
[27] I.J. Parkinson, J.A. Pearce, Peridotites from the Izu-Bonin–Mariana forearc (ODP leg 125): evidence for mantle melting and melt-mantle interaction in a supra-subduction zone setting, J. Petrol. 39 (1998) 1577–1618.
[28] J.A. Pearce, P.F. Baker, S.J. Edwards, I.J. Parkinson, P.T. Leat, Geochemistry and tectonic significance of peridotites from the South Sandwich arc-basin system, South Atlantic, Contrib. Mineral. Petrol. 139 (2000) 36–53.
[29] A. Tommasi, B. Tikoff, A. Vauchez, Upper mantle tectonics: three-dimensional deformation, olivine crystallographic fabrics and seismic properties, Earth Planet. Sci. Lett. 168 (1999) 173–186.
[30] S.J. Mackwell, D.L. Kohlsted, M.S. Paterson, Role of water in the deformation of olivine single-crystals, J. Geophys. Res. 90 (1985) 11,319–311,333.
[31] Q. Bai, S.J. Mackwell, D.L. Kohlstedt, High-temperature creep of olivine single crystals. 1. Mechanical results for buffered samples, J. Geophys. Res. 96 (1991) 2441–2463.
[32] A. Nicolas, F. Boudier, J.L. Bouchez, Interpretation of peridotite structures from ophiolitic and oceanic environments, Am. J. Sci. 280 (1980) 192–210.
[33] D. Cassard, Structure et origine des gisements de chromite du Massif du Sud Ophiolites de Nouvelle Caledonie), Thèse de 3ème Cycle, Université de Nantes, 1980.
[34] G. Suhr, Evaluation of upper mantle microstructures in the Table Mountain massif (Bayof Islands Ophiolite), J. Struct. Geol. 15 (1993) 1273–1292.
[35] F. Boudier, A. Nicolas, Nature of the Moho transition zone in the Oman ophiolite, J. Petrol. 36 (1995) 777–796.
[36] A. Tommasi, M. Godard, G. Coromina, J.-M. Dautria, H. Barsczus, Seismic anisotropy and compositionally induced velocity anomalies in the lithosphere above mantle plumes: a petrological and microstructural study of mantle xenoliths from French Polynesia, Earth Planet. Sci. Lett. 227 (2004) 539–556.
[37] D. Mainprice, M. Humbert, Methods of calculating petrophysical properties from lattice preferred orientation data, Surv. Geophys. 15 (1994) 575–592.
[38] E.H. Abramson, M. Brown, L.J. Slutsky, J. Zaug, The elastic constants of San Carlos olivine up to 17 GPa, J. Geophys. Res. 102 (1997) 12,252–12,263.
[39] M. Chai, J.M. Brown, L.J. Slutsky, The elastic constants of an aluminous orthopyroxene to 12.5 GPa, J. Geophys. Res. 102 (1997) 14,779–14,785.
[40] D.G. Isaak, O.L. Anderson, R.E. Cohen, The relationship between shear and compressional velocities at high pressures: reconciliation of seismic tomography and mineral physics, Geophys. Res. Lett. 19 (1992) 741–744.
[41] M. Spiegelman, P.B. Kelemen, E. Aharonov, Causes and consequences of flow organization during melt transport: the reaction infiltration instability in compactible media, J. Geophys. Res. 106 (2001) 2061–2077.
[42] U.H. Faul, Permeability of partially molten upper mantle rocks from experiments and percolation theory, J. Geophys. Res. 102 (1997) 10,299–10,311.
[43] H.S. Waff, U.H. Faul, Effects of crystalline anisotropy on fluid distribution in ultramafic partial melts, J. Geophys. Res. 97 (1992) 9003–9014.
[44] Y. Takei, Deformation-induced grain boundary wetting and its effects on the acoustic and rheological properties of partially molten rock analogue, J. Geophys. Res. 110 (2005) 1–24.
[45] B.K. Holtzman, N.J. Groebner, M.E. Zimmerman, S.B. Ginsberg, D.L. Kohlstedt, Stress-driven melt segregation in partially molten

rocks, Geochem. Geophys. Geosyst. 4 (2003) 1–26, doi:10.1029/2001GC000258.
[46] K.M. Fischer, M.J. Fouch, D.A. Wiens, M.S. Boettcher, Anisotropy and flow in Pacific subduction zone back-arcs, Pure Appl. Geophys. 151 (1998) 463–475.
[47] C.A. Currie, J.F. Cassidy, R.D. Hyndman, M.G. Bostock, Shear wave anisotropy beneath the Cascadia subduction zone and western North American craton, Geophys. J. Int. 157 (2004) 341–353.
[48] X. Yang, K.M. Fischer, G.A. Abers, Seismic anisotropy beneath the Shumagin Island segment of the Aleutian–Alaska subduction zone, J. Geophys. Res. 100 (1995) 18,165–118,177.
[49] S. Wiemer, G. Tytgat, M. Wyss, U. Duenkel, Evidence for shear-wave anisotropy in the mantle wedge beneath south central Alaska, Bull. Seismol. Soc. Am. 89 (1999) 1313–1322.
[50] A. Brisbourne, G. Stuart, J.M. Kendall, Anisotropic structure of the Hikurangi subduction zone, New Zealand; integrated interpretation of surface-wave and body-wave observations, Geophys. J. Int. 137 (1999) 214–230.
[51] V. Peyton, V. Levim, J. Park, M. Brandon, J. Lees, E. Gordeev, A. Ozerov, Mantle flow at a slab edge: seismic anisotropy in the Kamchatka region, Geophys. Res. Lett. 28 (2001) 379–382.
[52] G.P. Smith, D.A. Wiens, K.M. Fischer, L.M. Dorman, S.C. Webb, J.A. Hildebrand, A complex pattern of mantle flow in the Lau backarc, Science 292 (2001) 713–716.
[53] D. Mainprice, A.T., H. Couvy, P. Cordier, D.J. Frost, Pressure sensitivity of olivine slip systems and seismic anisotropy of the Earth's upper mantle, Nature 233 (2005) 731–733, doi:10.1038/nature03266.
[54] M.J. Fouch, K.M. Fischer, Mantle anisotropy beneath northwest Pacific subduction zones, J. Geophys. Res. 101 (1996) 15987–16002.
[55] R.-J. Rau, W.-T. Liang, H. Kao, B.-S. Hunag, Shear-wave anisotropy beneath the Taiwan orogen, Earth Planet. Sci. Lett. 177 (2000) 177–192.
[56] S. Civelo, L. Margheriti, Toroidal mantle flow around the Calabrina slab (Italy) from SKS splitting, Geophys. Res. Lett. 31 (2004) L10601, doi:10.1029/2004GL019607.
[57] K. Gledhill, D. Gubbins, SKS splitting and the seismic anisotropy of the mantle beneath the Hikurangi subduction zone, New Zealand, Phys. Earth Planet. Inter. 95 (1996) 227–236.
[58] L.T. Pinero, J. Lowman, J.M. Kendall, Comparisons of numerical simulations of mantle flow and seismic anisotropy in a model including a plate boundary transition region from subduction to transform to subduction, Eos, Trans., Am. Geophys. Union 83 (2002) F1364.
[59] J.V. Ross, The internal fabric of an alpine peridotite near Pinchi Lake, central British Columbia, Can. J. Earth Sci. 14 (1977) 32–44.